

2016-02-01

Is the Troodos ophiolite (Cyprus) a complete, transform fault-bounded Neotethyan ridge segment?

Morris, A

<http://hdl.handle.net/10026.1/5069>

10.1130/G37529.1

GEOLOGY

Geological Society of America

All content in PEARL is protected by copyright law. Author manuscripts are made available in accordance with publisher policies. Please cite only the published version using the details provided on the item record or document. In the absence of an open licence (e.g. Creative Commons), permissions for further reuse of content should be sought from the publisher or author.

Morris A & Maffione M 2016 'Is the Troodos ophiolite (Cyprus) a complete, transform fault-bounded Neotethyan ridge segment?' *GEOLOGY* 44, (3) 199-202

The published version of this paper is available at:

<http://geology.gsapubs.org/content/44/3/199.abstract?sid=36dba13e-7913-47b8-a6e7-ead143a94a26>

Publisher: GSA
Journal: GEOL: Geology
DOI:10.1130/G37529.1

1 Is the Troodos ophiolite (Cyprus) a complete, transform
2 fault–bounded Neotethyan ridge segment?

3 **Antony Morris¹ and Marco Maffione²**

4 *¹School of Geography, Earth and Environmental Sciences, Plymouth University, Drake
5 Circus, PL4 8AA Plymouth, UK*

6 *²Department of Earth Sciences, Utrecht University, Heidelberglaan 2, 3584 CS Utrecht,
7 Netherlands*

8 **ABSTRACT**

9 We report new paleomagnetic data from the sheeted dike complex of the Troodos
10 ophiolite (Cyprus) that indicate a hitherto unrecognized oceanic transform fault system
11 marks its northern limit. The style, magnitude and scale of upper crustal fault block
12 rotations in the northwestern Troodos region mirror those observed adjacent to the well-
13 known Southern Troodos Transform Fault Zone along the southern edge of the ophiolite.
14 A pattern of increasing clockwise rotation toward the north, coupled with consistent
15 original dike strikes and inclined net rotation axes across this region, is compatible with
16 distributed deformation adjacent to a dextrally slipping transform system with a principal
17 displacement zone just to the north of the exposed ophiolite. Combined with existing
18 constraints on the spreading fabric, this implies segmentation of the Troodos ridge system
19 on length scales of ~40 km, and suggests that a coherent strip of Neotethyan lithosphere,
20 representing a complete ridge segment bounded by transforms, has been uplifted to form
21 the currently exposed Troodos ophiolite. Moreover, the inferred length scale of the ridge
22 segment is consistent with formation at a slow-spreading rate during Tethyan seafloor

23 spreading and with a supra-subduction zone environment, as indicated by geochemical
24 constraints.

25 **INTRODUCTION**

26 The Troodos Complex of Cyprus is one of the world's best preserved ophiolites
27 (Gass, 1968; Moores and Vine, 1971). It formed during the Late Cretaceous
28 (Cenomanian–Turonian, U–Pb age 90–92 Ma; Mukasa and Ludden 1987) at a supra-
29 subduction zone spreading axis within the Neotethyan Ocean (Pearce, 2003), and consists
30 of a complete Penrose pseudostratigraphy disposed in a domal structure as a result of
31 focused Late Pliocene–Recent uplift (Robertson, 1990). Previous paleomagnetic and
32 structural analyses, focused on central and eastern Troodos (Clube and Robertson, 1986;
33 Bonhommet et al., 1988; Allerton, 1989a; MacLeod et al., 1990; Morris et al., 1990),
34 identified preservation of a fossil oceanic spreading ridge-transform fault system,
35 allowing models of transform tectonics to be developed and tested (Allerton, 1989b;
36 MacLeod et al., 1990; Gass et al., 1991). This Southern Troodos Transform Fault Zone
37 (STTFZ) (MacLeod and Murton, 1993) is characterized by differential clockwise
38 rotations around inclined axes of small (≤ 1 km), upper crustal fault blocks adjacent to a
39 dextrally-slipping transform, active during Late Cretaceous seafloor spreading (Clube and
40 Robertson, 1986; Bonhommet et al., 1988; Allerton, 1989a; MacLeod et al., 1990; Morris
41 et al., 1990; Scott et al., 2013; Cooke et al., 2014). Variable, shearing-induced rotations
42 resulted in tectonic disruption of the trend of sheeted dikes that originally intruded with a
43 consistent NW-SE strike (present-day coordinates; Allerton and Vine, 1987; Allerton,
44 1989a). The western limit of these distributed, localized rotations along the STTFZ

45 defines a fossil ridge-transform intersection (MacLeod et al., 1990) that aligns with the
46 inferred main spreading axis of the Solea graben (Hurst et al., 1992) to the north.

47 Here we present an analysis of net tectonic rotations in sheeted dikes to the west
48 of the Solea axis, a region representing ~40% of the total spreading-parallel width of the
49 exposed sheeted dike complex but where no previous systematic studies have been
50 undertaken. Dikes in this region also have variable present-day orientations suggesting
51 significant fault block rotations. Paleomagnetic analysis using a net tectonic rotation
52 approach allows determination of the initial strike of these dikes and assessment of the
53 pattern of tectonic rotations, providing new information on the spreading structure and
54 significance of this paleomagnetically unexplored part of the ophiolite.

55 **DIKE ORIENTATIONS, SAMPLING AND PALEOMAGNETIC DATA**

56 Surprisingly, given decades of international interest in the tectonic evolution of
57 Troodos, the sheeted dike complex of the northwestern domain of the ophiolite has
58 received only minor attention, with limited mapping of dike trends or fault zones (Cooke
59 et al., 2014) and paleomagnetic data only reported previously from two isolated sites
60 (Morris et al., 1998). However, road-cut sections offer near-continuous exposure of
61 sheeted dikes, which have been shown elsewhere in the ophiolite to carry stable, early,
62 seafloor spreading-related magnetic remanences (e.g., Allerton and Vine, 1987;
63 Bonhommet et al., 1988; Hurst et al., 1992) that pre-date deformation (Morris, 2003;
64 Morris et al., 2006) and may therefore be used as markers for tectonic rotation.

65 Field structural analysis from an ~30 km transect along the Pachyammos-Stavros
66 tis Psokas-Lysos road in the western Troodos (Fig. 1) reveals distinct differences in dike
67 orientation as the northern edge of the exposed ophiolite is approached: a southern

68 domain with generally N-S–striking dikes (mean strike/dip = $173^{\circ}/53^{\circ}$; $\alpha_{95} = 7.4^{\circ}$)
69 changes northward to a domain with ENE-WSW–striking dikes (mean strike/dip =
70 $237^{\circ}/48^{\circ}$; $\alpha_{95} = 10.4^{\circ}$) (Fig. DR1 in the GSA Data Repository¹).

71 Paleomagnetic samples were collected along this transect at 23 sites in sheeted
72 dikes. At each site, eight to ten oriented cores were drilled from adjacent dikes with
73 consistent orientation, one core per dike, to maximize averaging of secular variation.
74 Mean dike orientations and associated errors (α_{95}) at each site were obtained by
75 averaging structural measurements from each sampled dike. At five sites (WT03, WT05,
76 WT09, WT12, and WT14), single, discrete dikes were observed to obliquely cut across
77 the sheeted sequences. These were sampled separately (sites WT04, WT06, WT10,
78 WT13, and WT15) but proved to have magnetization directions identical to the host
79 sheeted dikes (Table DR1 in the Data Repository). They demonstrably were not
80 emplaced vertically and hence cannot be used in tectonic analyses. The in situ
81 remanences from all sites are reported (Table DR1), but only results from sheeted dikes
82 are discussed hereafter.

83 Standard paleomagnetic laboratory analyses (see the Data Repository) yielded
84 statistically well-defined site magnetization vectors (SMVs; Table DR1), after removal of
85 minor low stability viscous overprints (Fig. DR2a). Paleosecular variation of the
86 geomagnetic field is well-represented at 20 sites, according to the criteria of Deenen et al.
87 (2011) ($A_{95\min} < A_{95} < A_{95\max}$; Table DR1), supporting a primary origin of the remanence.
88 At the remaining three sites (WT18, WT19, WT20) paleosecular variation is under-
89 represented (i.e., $A_{95} < A_{95\min}$), probably due to rapid, near-simultaneous acquisition of
90 thermoremanent magnetization by sampled dikes.

91 The Troodos ophiolite experienced bulk $\sim 90^\circ$ counterclockwise rotation as an
92 oceanic microplate after cessation of seafloor spreading (Clube and Robertson, 1986;
93 Morris et al., 1990). West-directed remanences of upper crustal units away from zones of
94 localized deformation (i.e., away from the STTFZ) reflect this plate-scale rotation
95 (Moores and Vine, 1971; Clube et al., 1985; Morris et al., 2006) and define the so-called
96 ‘Troodos magnetization vector’ reference direction (TMV; declination/inclination =
97 $274^\circ/36^\circ$, $\alpha_{95} = 7.0^\circ$; Clube and Robertson, 1986). SMVs from the majority of sites show
98 consistent WNW directions with shallow-moderate inclinations that are statistically
99 different to the TMV (Fig. DR2b), demonstrating localized rotations of these units.
100 Exceptions are sites WT09 and WT26 where SMVs are statistically indistinguishable
101 from the TMV (Table DR1). However, moderate dips of dikes at these sites indicate that
102 some deformation has occurred.

103 **NET TECTONIC ROTATION ANALYSIS**

104 Paleomagnetic data are commonly interpreted tectonically by rotating sampled
105 units (and associated remanence vectors) to a local paleohorizontal or paleovertical
106 around present-day, strike-parallel axes. Such standard tilt corrections arbitrarily divide
107 the total deformation at a site into a vertical axis rotation followed by a tilt. This approach
108 is inadequate in sheeted dike terrains where components of rotation around dike-normal
109 axes do not result in observable changes in dike orientation (Borradaile, 2001; Morris and
110 Anderson, 2002). In these settings, it is more appropriate to calculate the single net
111 tectonic rotation around an inclined axis at a site that restores the SMV to an appropriate
112 reference direction and observed dike margins back to the paleovertical.

113 Here we apply an algorithm devised by Allerton and Vine (1987), and
114 subsequently applied in Troodos and other ophiolites (Allerton, 1989a; Morris et al.,
115 1990, 1998; Morris and Anderson, 2002; Hurst et al., 1992; Inwood et al., 2009), that
116 yields the azimuth and plunge of the net rotation axis, the magnitude and sense of
117 rotation, and the initial dike orientation (see the Data Repository). Following previous
118 studies (e.g., Allerton and Vine, 1987; Allerton, 1989a; Morris et al., 1998), we use the
119 TMV as a reference direction, representing the regional magnetization direction of the
120 Troodos ophiolite after microplate rotation. Hence, dikes are restored to primary
121 orientations that exclude the effects of microplate rotation, allowing comparison with
122 elements of the Troodos spreading structure established in the current geographic
123 reference frame.

124 Net tectonic rotation analysis at all sites yield two solutions capable of restoring
125 dikes to the paleovertical (Table DR2). Solutions providing NW-SE initial dike strikes
126 show systematic clockwise rotations (looking in the direction of the rotation pole
127 azimuth) and comparable orientations of rotation axes (Fig. 1; Fig. DR3; Table DR2).
128 Alternate solutions giving E-W or NE-SW initial dike strikes yield variable senses of
129 rotation (Table DR2), which are unlikely. Moreover, solutions yielding NW-SE strikes
130 have been accepted in previous studies (Allerton, 1989a; Morris et al., 1998) in areas of
131 the ophiolite where it was possible to show that alternate solutions restored associated
132 lavas to geological implausible initial orientations. NW-SE–striking solutions have been
133 chosen, therefore, as preferred solutions in this study (Table DR2). Permissible rotation
134 poles are well-clustered at most sites (Fig. DR4), indicating that calculated net tectonic
135 rotation solutions based on mean input vectors are reliable and can be used for tectonic

136 interpretation. Conversely, four sites (WT11, WT12, WT14, and WT26) showing larger
137 scatter of permissible rotation poles (Fig. DR4; Table DR2) have been discarded from
138 further analyses.

139 While rotation poles have comparable orientations across the study area, rotation
140 magnitudes are highly variable (Fig. 1; Table DR2; Fig. DR5) and fall into two broad
141 domains (Fig. 1; Fig. DR3): a northern area containing seven sites characterized by very
142 large ($>90^\circ$) rotations, and a southern area containing 12 sites characterized by moderate
143 ($<80^\circ$) rotations. Overall, net rotation magnitudes progressively decrease southward with
144 a rapid change in the first ~10 km from the northern edge of the study area. Importantly,
145 consistent initial dike orientations are found for all sites (Fig. 1, inset), despite highly
146 variable present-day orientations (Fig. DR1). This demonstrates that dikes were emplaced
147 with common NW-SE strikes (relative to present-day north) and were subsequently
148 disrupted by variable tectonic rotations of fault blocks. The absence of any major faults in
149 this region suggests that deformation was distributed, with rotations likely to be
150 accommodated by displacement on minor faults (Peacock et al., 1998).

151 **COMPARISON WITH THE SOUTHERN TROODOS TRANSFORM FAULT** 152 **ZONE**

153 The characteristics of rotational deformation in the study area (common initial
154 dike orientations, rotation around inclined axes, and progressive change in rotation
155 magnitude from north to south) are remarkably similar to those documented previously in
156 the region adjacent to the STTFZ. Dikes to the east of the Solea graben progressively
157 swing from NNW-SSE through NE-SW to ENE-WSW strikes across an ~10-km-wide
158 zone of distributed deformation as the STTFZ is approached (Fig. 1). This reflects

159 systematically clockwise but variable local rotations of initially NW-SE striking dikes
160 (relative to present-day north) during dextral slip along the transform (Clube and
161 Robertson, 1986; Bonhommet et al., 1988; Allerton, 1989a; MacLeod et al., 1990; Scott
162 et al., 2013). No major faults exist within this zone of rotation north of the STTFZ, again
163 indicating distributed deformation. Dikes within our study area mirror this pattern on a
164 similar length scale, with NW-SE initial emplacement and subsequent rotations resulting
165 in a marked variation in present-day orientations (from N-S to ENE-WSW strikes moving
166 northward), but in this case, with the largest rotations recorded in the northernmost sites.

167 **DISCUSSION**

168 The evidence for consistent clockwise rotations of sheeted dikes around inclined
169 axes with systematic variations in rotation magnitude from north to south across the study
170 area precisely matches the style and scale of transform-related deformation observed in
171 the STTFZ. The rotations observed in NW Troodos cannot be attributed to post-seafloor
172 spreading tectonics. The dominant neotectonic structure in this region is the Polis graben
173 to the west of the study area, which formed in the Miocene by ENE-WSW extension,
174 driven by subduction roll-back and trench migration (Payne and Robertson, 1995).
175 Structures associated with this event are not observed in the study area and, in any case,
176 could only account for minor tilting. The most significant earlier post-spreading tectonic
177 event affecting the ophiolite was paleorotation of the Troodos microplate, which initiated
178 in the Late Cretaceous and ended in the Eocene (Moores and Vine, 1971; Clube and
179 Robertson, 1986). A post-accretion phase of stretching related to this event has been
180 documented in the eastern part of the Limassol Forest Complex, within the STTFZ
181 (MacLeod, 1990). This led to development of a low angle extensional detachment fault

182 system (the Akapnou Forest Décollement; MacLeod, 1990) which was founded upon,
183 and reused, earlier transform-related structures. However, there is no evidence for post-
184 spreading extensional structures in NW Troodos, and, although their location is uncertain,
185 microplate boundaries must lie to the W of the Akamas peninsula (Fig. 1), which
186 demonstrably rotated as part of the microplate (Clube and Robertson, 1986; Morris et al.,
187 1998).

188 We propose, therefore, that clockwise tectonic rotations in NW Troodos are
189 instead related to distributed deformation adjacent to a dextrally slipping “Northern
190 Troodos Transform Fault Zone” (NTTFZ), with a principal displacement zone located
191 just to the N of the exposed ophiolite (Fig. 2). Clockwise rotations around inclined axes
192 plunging to the NW are likely due to the combined effects of rotation induced by shear
193 along the transform and tilting during seafloor spreading–related extension. This latter
194 component may reflect off-axis amagmatic extension, as inferred by Cooke et al. (2014)
195 from a structural analysis of the north Troodos margin just to the east of our study area.
196 We suggest an E-W trend for the NTTFZ, parallel to the Arakapas Fault. A WNW-ESE
197 strike parallel to the northern margin of the exposed ophiolite is precluded by net tectonic
198 rotation data from dikes in the Solea graben (Hurst et al., 1992) that show simple tilting
199 around horizontal axes and no evidence for a transform influence.

200 Together, the NTTFZ and STTFZ delineate the limits of an ~40-km-long Solea
201 spreading segment. This suggests that the Troodos spreading system was characterized by
202 short segments with transform offsets of similar or longer length-scale. This model (Fig.
203 2A) can also explain the presence of extrusive rocks in the northern Akamas peninsula
204 that have geochemical signatures similar to transform active sequences in the STTFZ

205 (Murton, 1990), an observation that is difficult to account for if the STTFZ represents the
206 only oceanic transform system preserved in the Troodos ophiolite (Morris et al., 1998).
207 This spreading geometry can account for the pronounced E-W elongation of the exposed
208 Troodos ophiolite, as it suggests that major transform/fracture zone structures mark both
209 its northern and southern limits.

210 The length scale of the Solea spreading segment, bounded by the NTTTFZ and
211 STTFZ, is similar to that observed in several modern supra-subduction zone systems (for
212 example, in the Andaman Sea (Fig. 2B), the Manus Basin, and the East Scotia Ridge;
213 Moores et al., 1984; Davies, 2012; Barker, 2001). This is consistent with geochemical
214 evidence (e.g., Pearce, 2003) that indicates formation of the Troodos ophiolite in a supra-
215 subduction zone environment, and supports an earlier suggestion by Moores et al. (1984)
216 that the Troodos system was likely marked by short ridge segments. Finally, there have
217 been considerable differences in estimates of the spreading rate of the Troodos ridge
218 system, from slow (Abelson et al., 2001) to intermediate-fast spreading (e.g., Allerton
219 and Vine, 1987, 1990). A first-order constraint on this is provided by a systematic (but
220 nonlinear) relationship between segment length and spreading rate (Sandwell 1986;
221 Sandwell and Smith, 2009). Using this relationship, the length-scale of the Solea segment
222 indicates that the Troodos ophiolite formed by spreading at a slow rate (of <4 cm/year,
223 full rate).

224 **ACKNOWLEDGMENTS**

225 We thank Chun-Tak Chu for assistance in the field and for undertaking some of
226 the laboratory analyses, and Sarah Titus and an anonymous referee for helpful reviews.
227 Stereonets were produced using OSXStereonet (Cardozo and Allmendinger, 2013).

228 **REFERENCES CITED**

- 229 Abelson, M., Baer, G., and Agnon, A., 2001, Evidence from gabbro of the Troodos
230 ophiolite for lateral magma transport along a slow-spreading mid-ocean ridge:
231 Nature, v. 409, p. 72–75, doi:10.1038/35051058.
- 232 Allerton, S., 1989a, Fault block rotations in ophiolites: Results of palaeomagnetic studies
233 in the Troodos Complex, Cyprus, *in* Kissel, C., and Laj, C., eds., Palaeomagnetic
234 Rotations and Continental Deformation: NATO ASI Series C, v. 254, p. 393–410,
235 doi:10.1007/978-94-009-0869-7_24.
- 236 Allerton, S., 1989b, Distortions, rotations and crustal thinning at ridge-transform
237 intersections: Nature, v. 340, p. 626–628, doi:10.1038/340626a0.
- 238 Allerton, S., and Vine, F.J., 1987, Spreading structure of the Troodos ophiolite, Cyprus:
239 Some paleomagnetic constraints: Geology, v. 15, p. 593, doi:10.1130/0091-
240 7613(1987)15<593:SSOTTO>2.0.CO;2.
- 241 Allerton, S., and Vine, F.J., 1990, Palaeomagnetic and structural studies of the
242 southeastern part of the Troodos complex, *in* Malpas, J., et al., eds., Ophiolites:
243 Oceanic Crustal Analogues: Proceedings of the symposium "Troodos 1987",
244 Ministry of Agriculture and Natural Resources, Geological Survey Department,
245 Republic of Cyprus, Nicosia, Cyprus, p. 99–111.
- 246 Barker, P.F., 2001, Scotia sea regional tectonic evolution: Implications for mantle flow
247 and palaeocirculation: Earth-Science Reviews, v. 55, p. 1–39, doi:10.1016/S0012-
248 8252(01)00055-1.

- 249 Bonhommet, N., Roperch, P., and Calza, F., 1988, Paleomagnetic arguments for block
250 rotations along the Arakapas fault (Cyprus): *Geology*, v. 16, p. 422,
251 doi:10.1130/0091-7613(1988)016<0422:PAFBRA>2.3.CO;2.
- 252 Borradaile, G.J., 2001, Paleomagnetic vectors and tilted dikes: *Tectonophysics*, v. 333,
253 p. 417–426, doi:10.1016/S0040-1951(00)00296-1.
- 254 Cardozo, N., and Allmendinger, R.W., 2013, Spherical projections with OSXStereonet:
255 *Computers & Geosciences*, v. 51, p. 193–205, doi:10.1016/j.cageo.2012.07.021.
- 256 Clube, T.M.M., and Robertson, A.H.F., 1986, The palaeorotation of the Troodos
257 microplate, Cyprus, in the late Mesozoic-early Cenozoic plate tectonic framework of
258 the Eastern Mediterranean: *Surveys in Geophysics*, v. 8, p. 375–437,
259 doi:10.1007/BF01903949.
- 260 Clube, T.M.M., Creer, K.M., and Robertson, A.H.F., 1985, Palaeorotation of the Troodos
261 microplate, Cyprus: *Nature*, v. 317, p. 522–525, doi:10.1038/317522a0.
- 262 Cooke, A.J., Masson, L.P., and Robertson, A.H.F., 2014, Construction of a sheeted dyke
263 complex: evidence from the northern margin of the Troodos ophiolite and its
264 southern margin adjacent to the Arakapas fault zone: *Ophioliti*, v. 39, p. 1–30,
265 doi:10.4454/ofioliti.v39i1.426.
- 266 Davies, H.L., 2012, The geology of New Guinea -the cordilleran margin of the Australian
267 continent: *Episodes*, v. 35, p. 87–102.
- 268 Deenen, M.H.L., Langereis, C.G., van Hinsbergen, D.J.J., and Biggin, A.J., 2011,
269 Geomagnetic secular variation and the statistics of palaeomagnetic directions:
270 *Geophysical Journal International*, v. 186, p. 509–520, doi:10.1111/j.1365-
271 246X.2011.05050.x.

- 272 Gass, I.G., 1968, Is the Troodos massif of Cyprus a fragment of Mesozoic ocean floor?:
273 Nature, v. 220, p. 39–42, doi:10.1038/220039a0.
- 274 Gass, I.G., MacLeod, C.J., Murton, B.J., Panayiotou, A., Simonian, K.O., and
275 Xenophontos, C., 1991, Geological Map of the South Troodos Transform Fault Zone
276 at 1:25.000: Sheets 1 (west) and 2 (east): Nicosia, Cyprus Geological Survey
277 Department.
- 278 Hurst, S.D., Verosub, K.L., and Moores, E.M., 1992, Paleomagnetic constraints on the
279 formation of the Solea graben, Troodos ophiolite: Tectonophysics, v. 208, p. 431–
280 445, doi:10.1016/0040-1951(92)90439-D.
- 281 Inwood, J., Morris, A., Anderson, M.W., and Robertson, A.H.F., 2009, Neotethyan
282 intraoceanic microplate rotation and variations in spreading axis orientation:
283 Palaeomagnetic evidence from the Hatay ophiolite (southern Turkey): Earth and
284 Planetary Science Letters, v. 280, p. 105–117, doi:10.1016/j.epsl.2009.01.021.
- 285 MacLeod, C.J., 1990, Role of the Southern Troodos Transform Fault in the rotation of the
286 Cyprus microplate: Evidence from the Eastern Limassol Forest, *in* Malpas, J.,
287 Moores, E.M., Panayiotou, A., and Xenophontos, C., eds., Ophiolites: Oceanic
288 Crustal Analogues: Nicosia, Cyprus Geological Survey Department, p. 75–85.
- 289 MacLeod, C.J., and Murton, B.J., 1993, Structure and tectonic evolution of the Southern
290 Troodos Transform Fault Zone, Cyprus, *in* Prichard, H.M., et al., eds., Magmatic
291 Processes and Plate Tectonics: Geological Society, London, Special Publication 76,
292 p. 141–176, doi:10.1144/GSL.SP.1993.076.01.07.

- 293 MacLeod, C.J., Allerton, S., Gass, I.G., and Xenophontos, C., 1990, Structure of a fossil
294 ridge-transform intersection in the Troodos ophiolite: *Nature*, v. 348, p. 717–720,
295 doi:10.1038/348717a0.
- 296 Moores, E.M., and Vine, F.J., 1971, The Troodos Massif, Cyprus and other ophiolites as
297 oceanic crust: Evaluation and implications: *Philosophical Transactions of the Royal*
298 *Society of London*, v. 268, p. 443–467, doi:10.1098/rsta.1971.0006.
- 299 Moores, E.M., Robinson, P.T., Malpas, J., and Xenophontos, C., 1984, Model for the
300 origin of the Troodos massif, Cyprus, and other mideast ophiolites: *Geology*, v. 12,
301 p. 500–503, doi:10.1130/0091-7613(1984)12<500:MFTOOT>2.0.CO;2.
- 302 Morris, A., 2003, The Late Cretaceous palaeolatitude of the Neotethyan spreading axis in
303 the eastern Mediterranean region: *Tectonophysics*, v. 377, p. 157–178,
304 doi:10.1016/j.tecto.2003.08.016.
- 305 Morris, A., and Anderson, M.W., 2002, Palaeomagnetic results from the Baër-Bassit
306 ophiolite of northern Syria and their implication for fold tests in sheeted dyke
307 terrains: *Physics and Chemistry of the Earth*, v. 27, p. 1215–1222,
308 doi:10.1016/S1474-7065(02)00123-7.
- 309 Morris, A., Creer, K.M., and Robertson, A.H.F., 1990, Palaeomagnetic evidence for
310 clockwise rotations related to dextral shear along the Southern Troodos Transform
311 Fault, Cyprus: *Earth and Planetary Science Letters*, v. 99, p. 250–262,
312 doi:10.1016/0012-821X(90)90114-D.
- 313 Morris, A., Anderson, M.W., and Robertson, A.H.F., 1998, Multiple tectonic rotations
314 and transform tectonism in an intraoceanic suture zone, SW Cyprus: *Tectonophysics*,
315 v. 299, p. 229–253, doi:10.1016/S0040-1951(98)00207-8.

- 316 Morris, A., Anderson, M.W., Inwood, J., and Robertson, A.H.F., 2006, Palaeomagnetic
317 insights into the evolution of Neotethyan oceanic crust in the eastern Mediterranean:
318 Geological Society of London, Special Publications, v. 260, p. 351–372,
319 doi:10.1144/GSL.SP.2006.260.01.15.
- 320 Mukasa, S.B., and Ludden, J.N., 1987, Uranium-lead isotopic ages of plagiogranites from
321 the Troodos ophiolite, Cyprus, and their tectonic significance: *Geology*, v. 15,
322 p. 825, doi:10.1130/0091-7613(1987)15<825:U1AOPF>2.0.CO;2.
- 323 Murton, B.J., 1990, Was the Southern Troodos Transform Fault a victim of microplate
324 rotation? *in* Malpas, J., et al., eds., *Ophiolites: Oceanic Crustal Analogues*: Nicosia,
325 Cyprus Geological Survey Department, p. 87–98.
- 326 Payne, A.S., and Robertson, A.H.F., 1995, Neogene supra-subduction zone extension in
327 the Polis graben system, west Cyprus: *Journal of the Geological Society*, v. 152,
328 p. 613-628.
- 329 Peacock, D.C.P., Anderson, M.W., Morris, A., and Randall, D.E., 1998, Evidence for the
330 importance of ‘small’ faults on block rotation: *Tectonophysics*, v. 299, p. 1–13,
331 doi:10.1016/S0040-1951(98)00195-4.
- 332 Pearce, J.A., 2003, Supra-subduction zone ophiolites: The search for modern analogues,
333 *in* Dilek, Y., and Newcomb, S., eds., *Ophiolite Concept and the Evolution of*
334 *Geological Thought*: Geological Society of America Special Paper 373, p. 269–293,
335 doi:10.1130/0-8137-2373-6.269.
- 336 Robertson, A.H.F., 1990, Tectonic evolution of Cyprus, *in* Malpas, J., et al., eds.,
337 *Ophiolites: Oceanic Crustal Analogues*: Nicosia, Cyprus Geological Survey
338 Department, p. 235–252.

- 339 Sandwell, D.T., 1986, Thermal stress and the spacing of transform faults: *Journal of*
340 *Geophysical Research*, v. 91, p. 6405–6417, doi:10.1029/JB091iB06p06405.
- 341 Sandwell, D.T., and Smith, W.H.F., 2009, Global marine gravity from retracked Geosat
342 and ERS-1 altimetry: Ridge segmentation versus spreading rate: *Journal of*
343 *Geophysical Research. Solid Earth*, v. 114, B01411, doi:10.1029/2008JB006008.
- 344 Scott, C.P., Titus, S.J., and Davis, J.R., 2013, Using field data to constrain a numerical
345 kinematic model for ridge-transform deformation in the Troodos ophiolite, Cyprus:
346 *Lithosphere*, v. 5, p. 109–127, doi:10.1130/L237.1.

347 **FIGURE CAPTIONS**

348 Figure 1. Geological map of the Troodos ophiolite (Cyprus) showing the location of the
349 study area, and main structural features, such as the axis and edges of the Solea graben
350 (red lines), the Southern Troodos Transform Fault Zone (STTFZ), and the general
351 orientation of sheeted dikes (short black lines). The region in the study area characterized
352 by the most highly rotated dikes (north domain; see text) is shaded in gray. Inset: results
353 of net tectonic rotation analysis for the northern and southern domains of the study area,
354 shown as rose diagrams of initial dike orientations (left), contoured equal area
355 stereographic projections of permissible rotation axes (center), and frequency
356 distributions of rotation magnitudes (right).

357

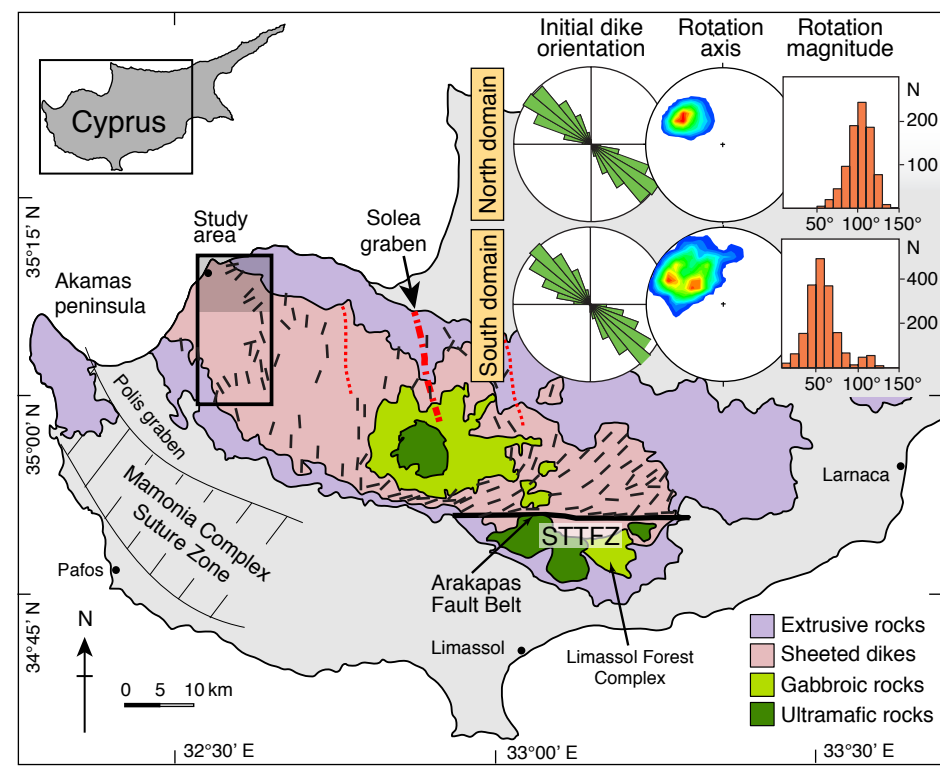
358 Figure 2. A: Proposed tectonic model for the origin of clockwise fault block rotations in
359 NW Troodos (Cyprus). Dark gray areas indicate the inferred locations where rotations
360 occur, at the inside corners of the two ridge-transform intersections (following the model
361 of Allerton, 1989b). Location of spreading axes to the north and south of the transform

362 faults are unconstrained and shown schematically by dotted lines. B: Outline tectonic
363 map of the Andaman Sea (from Moores et al., 1984). White dashed line encloses a region
364 where ridge segments have similar scale to that proposed for the Troodos spreading
365 system. Gray shading shows late Miocene or younger crust. Ruled area is accretionary
366 prism.

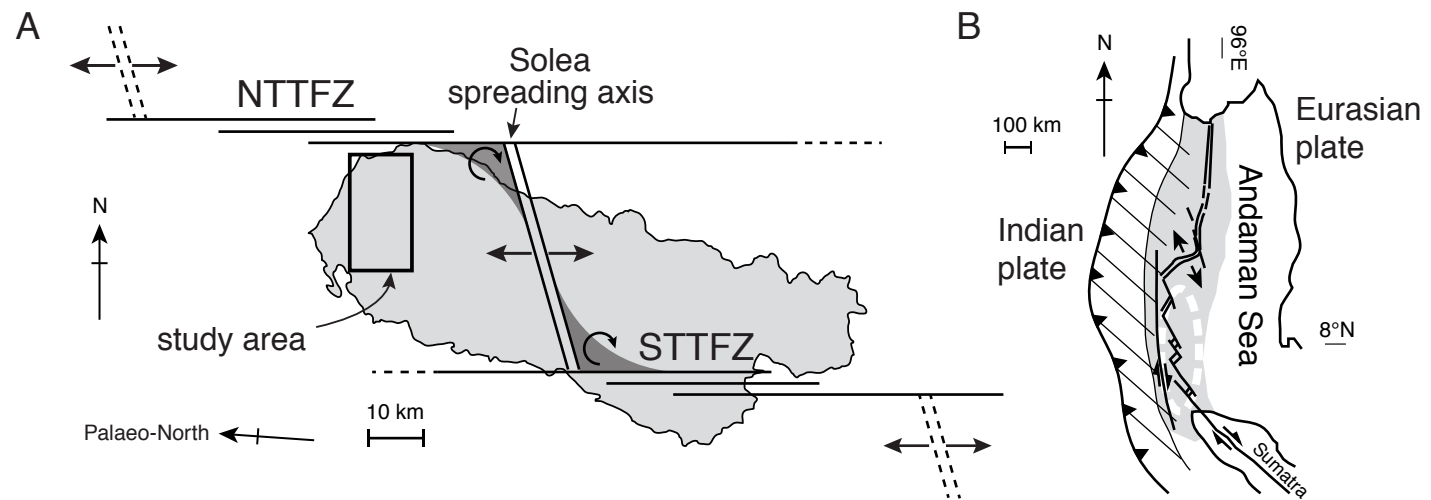
367

368 ¹GSA Data Repository item 2016xxx, xxxxxxxx, is available online at
369 www.geosociety.org/pubs/ft2016.htm, or on request from editing@geosociety.org or
370 Documents Secretary, GSA, P.O. Box 9140, Boulder, CO 80301, USA.

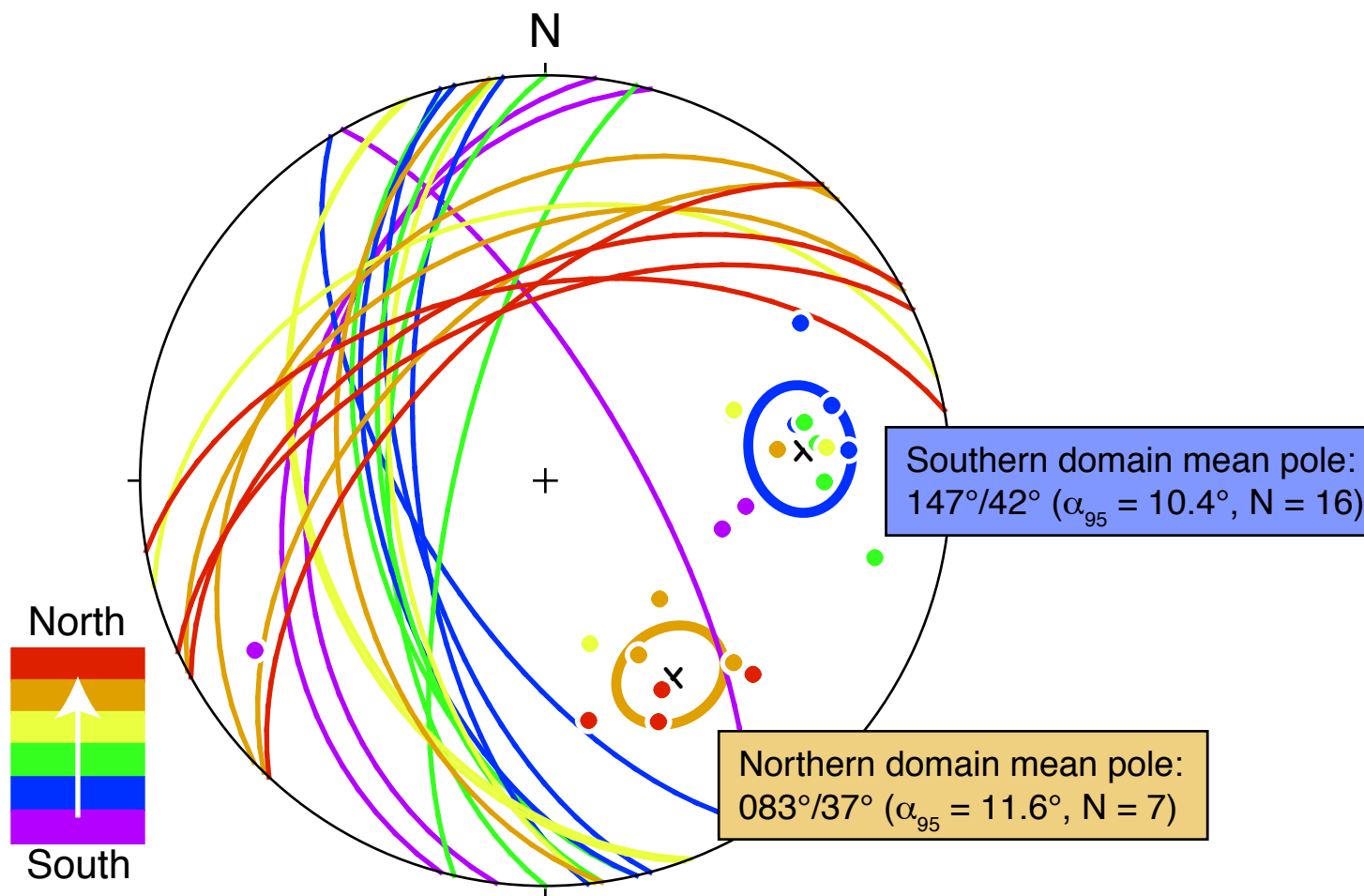
Morris and Maffione
Figure 1
Adobe Illustrator CS5, version 15.0.0



Morris and Maffione
Figure 2
Adobe Illustrator CS5, version 15.0.0



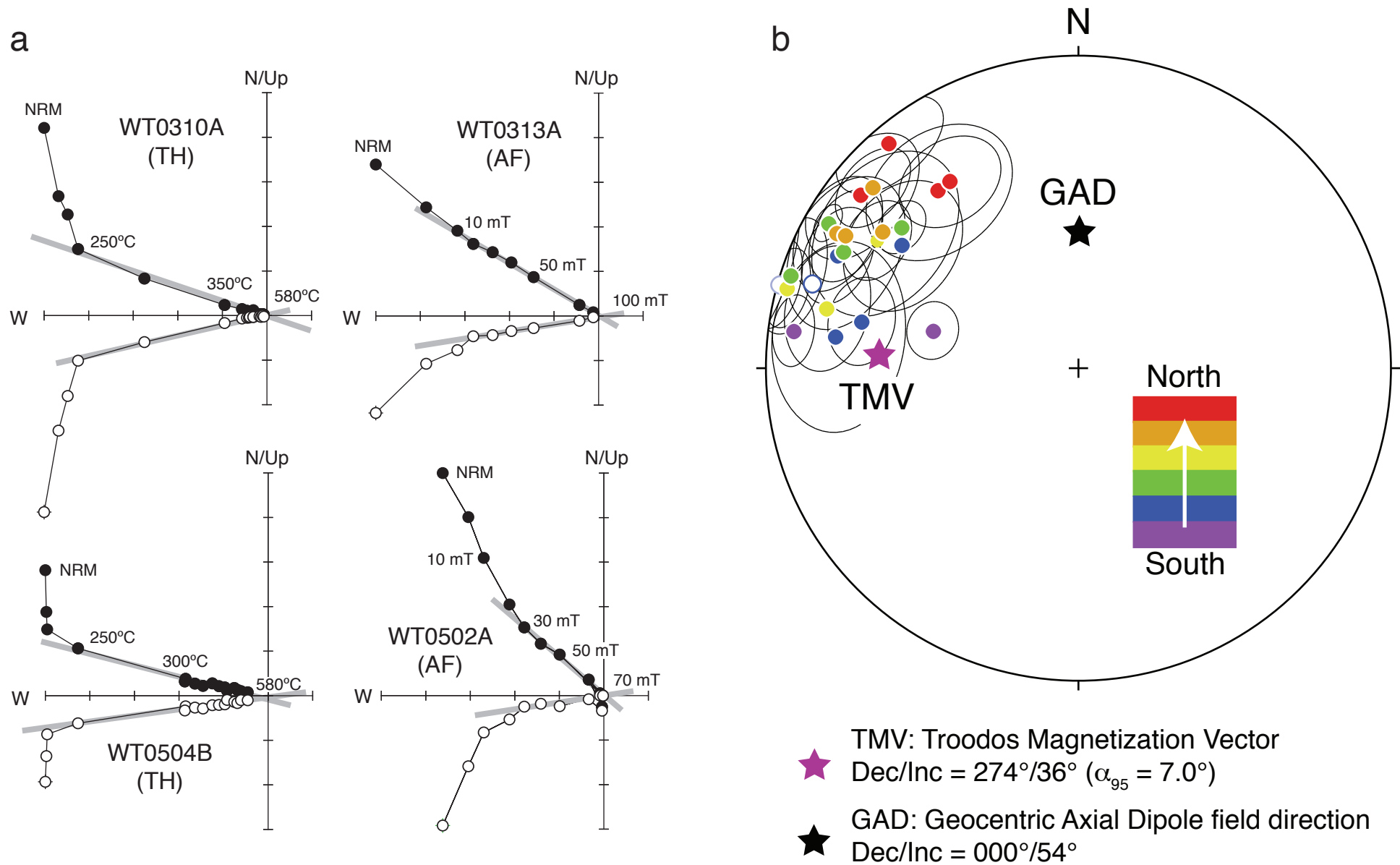
Morris and Maffione
Figure DR1
Adobe Illustrator CS5, version 15.0.0

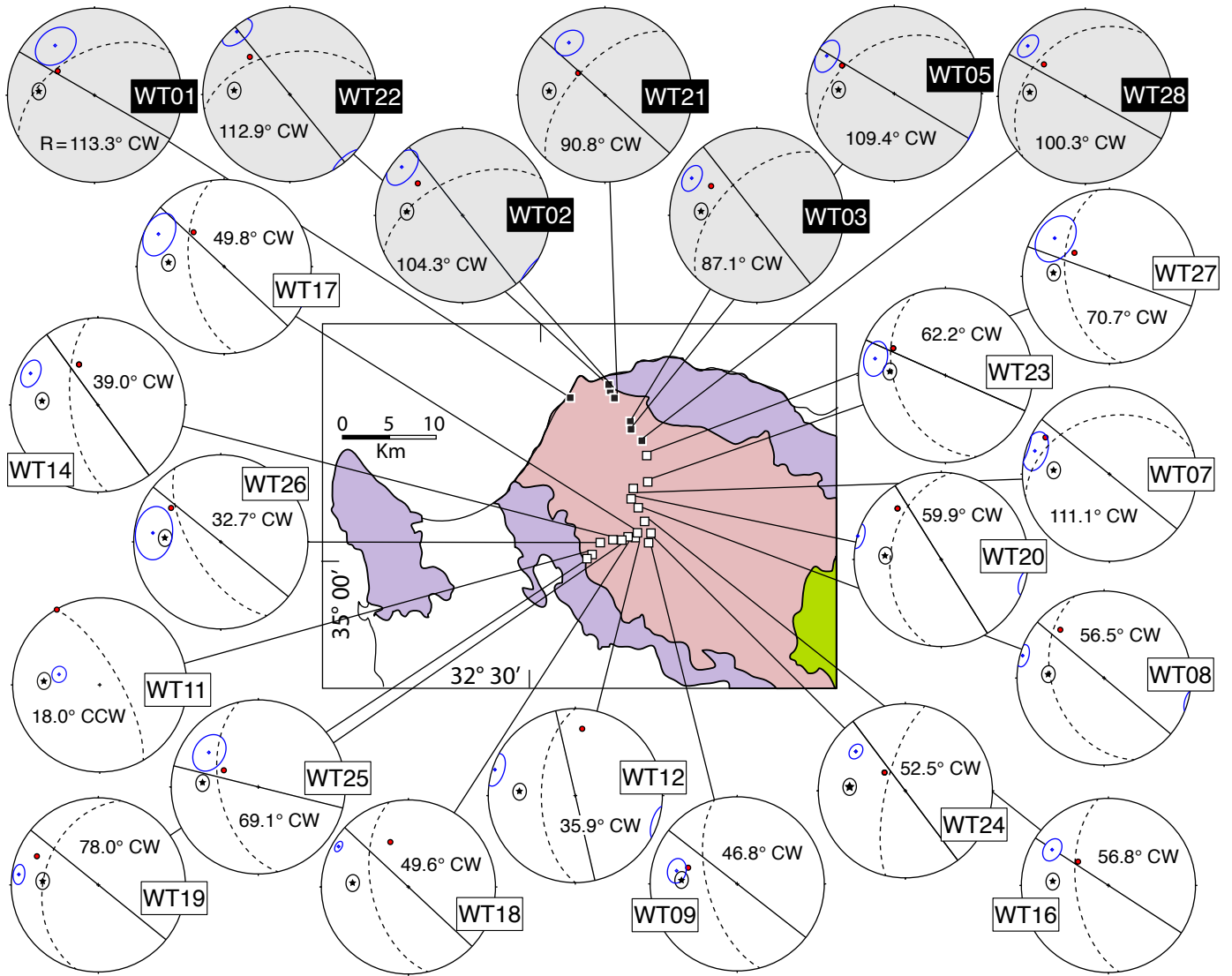


Morris and Maffione

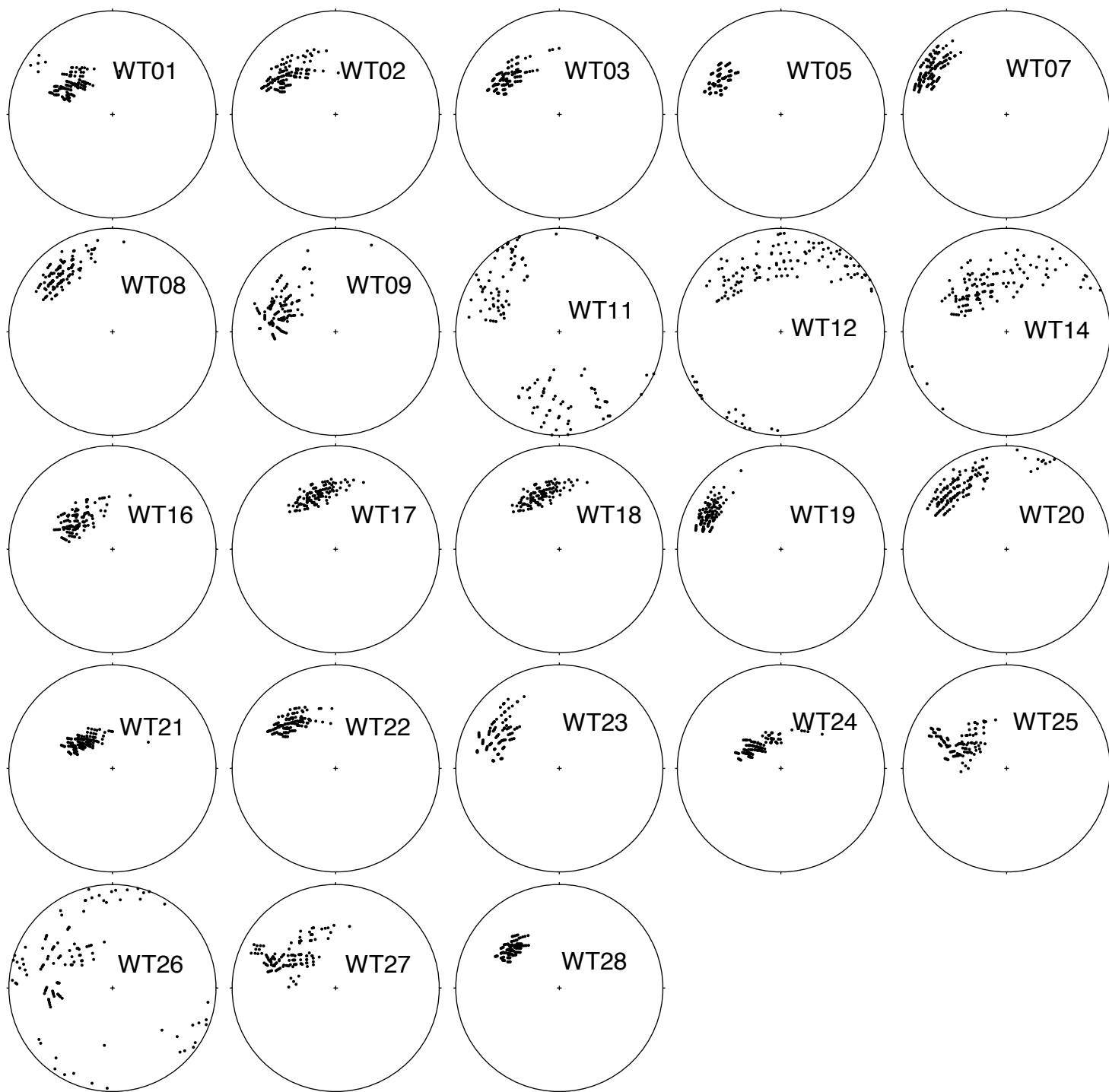
Figure DR2

Adobe Illustrator CS5, version 15.0.0

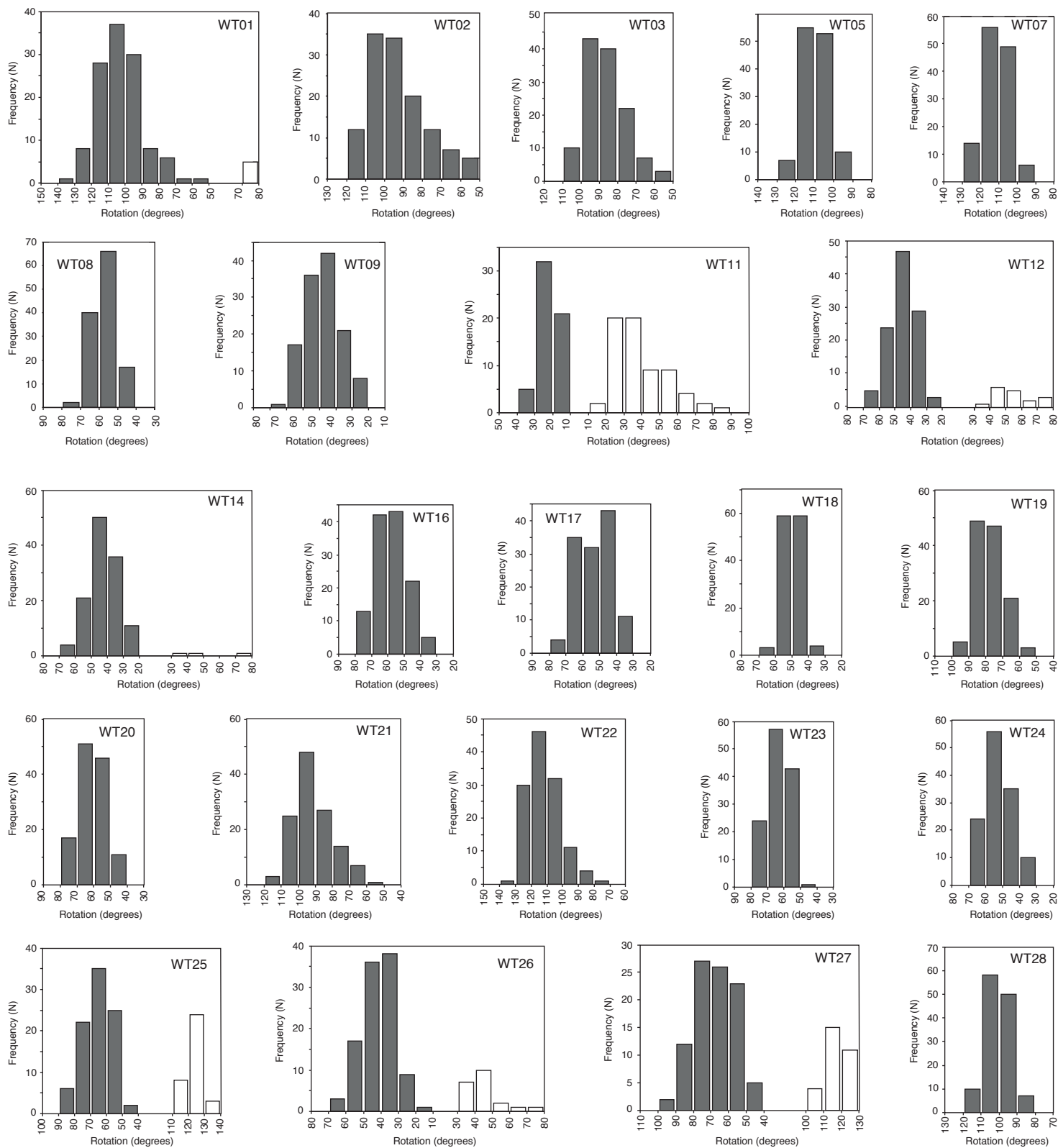




Morris and Maffione
Figure DR3
Adobe Illustrator CS5, version 15.0.0



Morris and Maffione
Figure DR4
Adobe Illustrator CS5, version 15.0.0



Data Repository – methods

1.1. Paleomagnetic analysis

Natural remanent magnetizations (NRMs) of samples were investigated via alternating field (AF) demagnetization using an AGICO LDA-3A demagnetizer in 12 incremental steps from 5 to 100 mT. One twin specimen per site was thermally demagnetized with 14-16 temperature increments from 100 to 580°C (or until complete demagnetization) to determine the blocking temperature(s) of the magnetic carriers. Magnetic remanences were measured at each AF or thermal demagnetization step using an AGICO JR-6A spinner magnetometer. Demagnetization data were displayed on orthogonal vector plots (Zijderveld, 1967), and remanence components were isolated via principal component analysis (Kirschvink, 1980) using Remasoft 3.0 software (Chadima and Hrouda, 2006). Site mean directions were evaluated using Fisherian statistics (Fisher, 1953) on virtual geomagnetic poles (VGPs) corresponding to the isolated characteristic remanent magnetizations (ChRMs). All VGPs at each site fell within the 45° cut-off recommended by Johnson et al. (2008). Paleomagnetic quality criteria proposed by Deenen et al. (2011) were adopted to estimate the reliability of the ChRM/VGP distribution at the site level. In particular, the VGP scatter (i.e., A_{95}) obtained at each site was compared to the expected scatter induced by paleosecular variation (PSV) of the geomagnetic field (i.e., $A_{95min} - A_{95max}$) to assess whether PSV was sufficiently represented in our datasets (Deenen et al., 2011). For values of $A_{95} < A_{95min}$ PSV is not adequately represented, indicating either insufficient time averaging of the geomagnetic field (i.e. sampled dikes were injected in a short period of time), or remagnetization. Conversely, values of $A_{95} > A_{95max}$ may

indicate additional (tectonic) processes responsible for the enhanced scatter of paleomagnetic directions.

1.2. Net tectonic rotation

Net tectonic rotation analysis describes the final (net) deformation at a paleomagnetic sampling site in terms of a single rotation about an inclined axis, which, in sheeted dike complexes, simultaneously restores dikes back to their initial (vertical) orientation and their *in situ* mean remanence to an appropriate reference direction. Net tectonic rotation solutions are expressed as the azimuth and plunge of the rotation axis, the magnitude and sense of the rotation, and the initial dike orientation. Key assumptions of this method (Allerton and Vine, 1987) are: (1) remanence was acquired before tilting; (2) an appropriate (coeval) reference magnetization direction may be found; (3) dikes were initially vertical; (4) no significant internal deformation has occurred.

Two solutions are generated if the dike can be restored to the vertical. In this case, additional geological evidence should be used to choose a preferred solution. If a dike cannot be restored to the vertical a single solution is obtained for the rotation axis that restores the dike to its steepest orientation. The uncertainties associated with the calculated net tectonic rotation parameters at each site are directly dependent on the errors associated with the reference magnetization vector, *in situ* remanence, and dike orientation. To quantify this uncertainty an iterative method was devised by Morris et al. (1998) and successfully applied to the study of the sheeted dikes from other areas of Troodos and other ophiolites. In this method, five potential values (mean value, plus four points located along the 95% ellipses of confidence) are selected for each of the three input vectors used for the analysis. The 125 combinations of input vectors (5

x 5 x 5) provide 125 individual permissible net tectonic rotation solutions at a site (that define an irregular envelope providing a first-order approximation of the 95% confidence region for rotation axes) together with a frequency distribution of associated rotation angles.

References

- Allerton, S., and Vine, F. J., 1987, Spreading structure of the Troodos ophiolite, Cyprus: Some paleomagnetic constraints: *Geology*, v. 15, no. 7, p. 593.
- Chadima, M., Hrouda, F., 2006, Remasoft 3.0 a user-friendly paleomagnetic data browser and analyzer. *Travaux Géophysiques XXVII*, 20–21.
- Deenen, M. H. L., Langereis, C. G., van Hinsbergen, D. J. J., and Biggin, A. J., 2011, Geomagnetic secular variation and the statistics of palaeomagnetic directions: *Geophysical Journal International*, v. 186, no. 2, p. 509-520.
- Fisher, R. A., 1953, Dispersion on a sphere: *Proc. R. Soc. London*, v. 217, p. 295-305.
- Johnson, C.L., et al., 2008, Recent investigations of the 0–5 Ma geomagnetic field recorded by lava flows: *Geochemistry, Geophysics, Geosystems*, v. 9, Q04032, doi.org/10.1029/2007GC001696.
- Kirschvink, J. L., 1980, The least-squares line and plane and the analysis of palaeomagnetic data: *Geophysical Journal, Royal Astronomical Society*, v. 62, no. 3, p. 699-718.
- Morris, A., Anderson, M.W., Robertson, A.H.F., 1998, Multiple tectonic rotations and transform tectonism in an intraoceanic suture zone, SW Cyprus: *Tectonophysics*, v. 299, no. 1-3, p. 229-253.
- Zijderveld, J. D. A., 1967, AC demagnetization of rocks: Analysis of results: *Methods in Paleomagnetism*, p. 254-286.

1 **Figure Captions (Data Repository)**

2

3 **Figure DR1.** Equal area stereographic projection (lower hemisphere) of in situ dike
4 orientations within the study area, displayed as planes (great circles) and poles (dots),
5 color-coded by increasing site latitude. Two regions characterized by different dike
6 orientation are recognized: a northern domain with NE-SW-trending dikes, and a
7 southern domain with mainly N-S-trending dikes. Cones of 95% confidence around
8 the dike poles calculated separately for the northern and southern domain demonstrate
9 statistically significant differences ($\sim 60^\circ$) between the mean dike orientations in the
10 two domains. Three sites in late dikes (see text) and two additional sites showing
11 inconsistent dike orientations, have been excluded from the computation of mean dike
12 orientations.

13

14 **Figure DR2.** (a) Representative orthogonal vector plots (in situ coordinates) for twin
15 specimens demagnetized thermally (TH) and using alternating fields (AF). Solid/open
16 circles are projections of the remanence vector onto the horizontal/vertical planes
17 respectively. Demagnetization steps are in $^\circ\text{C}$ or millitesla (mT). Gray lines are the
18 characteristic remanent magnetizations (ChRMs) isolated in each specimen. (b) Equal
19 area stereographic projection (lower hemisphere) of site mean directions (dots) and
20 associated α_{95} cones of confidence (gray ellipses) from all sites sampled, color-coded
21 by increasing site latitude. Colored/open symbols represent positive/negative
22 inclinations respectively. Purple star, Troodos magnetization vector (TMV;
23 declination/inclination = $274^\circ/36^\circ$, $\alpha_{95} = 7.0^\circ$; Clube and Robertson (1985)). Black
24 star, direction of the present geocentric axial dipole field (GAD) in Cyprus (D/I =
25 $000^\circ/54.6^\circ$).

26

27 **Figure DR3.** Equal area stereographic projections showing results of net tectonic
28 rotation analysis at all sampled sites. Gray/white projections and black/white squares
29 on the geological map indicate sites in the northern/southern domains, respectively
30 (see text); black stars, Troodos reference direction (TMV); blue dots, *in situ* site mean
31 remanence directions (with associated 95% cones of confidence); red dots, net
32 tectonic rotation axes; R, amount of rotation (CW, clockwise; CCW,
33 counterclockwise).

34

35 **Figure DR4.** Equal area stereographic projections showing the 125 permissible
36 rotation axes (black dots) computed by net tectonic rotation analysis at each sampling
37 site. The scatter of the permissible rotation axes provides a first-order estimate of the
38 error associated with the mean rotation axis calculated at each site.

39

40 **Figure DR5.** Histograms of the 125 permissible rotation magnitudes obtained at each
41 site. Dark gray and white bars indicate CW and CCW net rotation, respectively.

42

43 **Table DR1.** Paleomagnetic results from the sheeted dike complex of the western
44 Troodos ophiolite.^D Discrete dike. Dike orientation is expressed as strike/dip. $DP\alpha_{95}$,
45 95% cone of confidence around the calculated mean dike orientation. D, I, declination
46 and inclination of *in situ* site mean remanence. dD, dI, declination and inclination
47 error, respectively. k, α_{95} , precision parameter and 95% cone of confidence around the
48 site mean characteristic remanent magnetizations (ChRMs) after Fisher (1955). K,
49 A_{95} , precision parameter and 95% cone of confidence around the site mean virtual
50 geomagnetic pole (VGP). $A_{95\text{min}}$, $A_{95\text{max}}$, minimum and maximum value of A_{95}

51 expected from paleosecular variation (PSV) of the geomagnetic field, according to
52 Deenen et al. (2011). N, number of total samples used for the statistics.

53

54 **Table DR2.** Results of net tectonic rotation analysis in the sheeted dike complex of
55 the western Troodos ophiolite. Sites are listed in geographical order from north to
56 south. Both preferred (gray area) and alternate solutions are reported. For each
57 solution the azimuth (Az) and plunge of the rotation axis, the rotation angle (R) and
58 sense of rotation, and the initial dike strike and dip are listed. *, discarded sites (see
59 text).

60

Table DR1. Paleomagnetic results from the sheeted dike complex of the western Troodos ophiolite.

Site	Latitude (°N)	Longitude (°E)	Dyke str./dip	DP α_{95}	Mean remanence vector				k	α_{95}	K	A ₉₅	A _{95min}	A _{95max}	N
					D	dD	I	dI							
WT01	35°09'26.43"	32°32'32.08"	241/49	9.3	321.6	18.4	28.0	29.6	12.2	18.0	12.5	17.7	5.5	24.1	7
WT02	35°10'10.18"	32°35'29.97"	245/55	7.6	308.5	10.1	11.6	19.5	15.2	14.7	31.3	10.1	5.2	22.1	8
WT03	35°07'51.51"	32°36'51.82"	224/54	4.0	299.7	7.9	15.0	14.9	23.1	10.3	39.0	7.8	4.8	19.2	10
WT04 ^D	35°07'51.51"	32°36'51.82"	149/44	9.9	291.9	8.2	22.7	14.2	39.4	9.7	57.9	8.0	5.5	24.1	7
WT05	35°07'34.37"	32°36'50.88"	242/40	3.6	299.2	12.0	12.1	23.2	20.3	12.6	22.3	12.0	5.2	22.1	8
WT06 ^D	35°07'34.37"	32°36'50.88"	140/59	8.4	295.4	6.3	20.4	11.2	50.6	7.9	81.2	6.2	5.2	22.1	8
WT07	35°04'20.64"	32°37'0.476"	255/34	8.2	287.7	9.7	-11.3	18.7	15.7	14.4	34.2	9.6	5.2	22.1	8
WT08	35°03'18.11"	32°37'20.47"	160/40	7.8	285.4	5.2	3.4	10.3	53.0	7.7	115.6	5.2	5.2	22.1	8
WT09	35°01'19.87"	32°37'59.21"	165/62	8.9	282.2	7.7	29.5	12.2	31.5	10.0	56.4	7.4	5.2	22.1	8
WT10 ^D	35°01'19.87"	32°37'59.21"	035/80	5.0	291.2	6.2	26.9	10.2	52.2	7.7	84.8	6.0	5.2	22.1	8
WT11	35°00'34.41"	32°34'07.45"	330/72	8.9	284.5	9.2	50.1	8.8	62.6	7.1	49.8	7.9	5.2	22.1	8
WT12	35°01'39.39"	32°37'08.49"	180/58	9.3	287.9	9.3	3.4	18.6	24.5	11.4	36.1	9.3	5.2	22.1	8
WT13 ^D	35°01'39.39"	32°37'08.49"	143/75	5.0	294.1	6.0	15.5	11.2	61.8	7.7	104.9	5.9	5.5	24.1	7
WT14	35°01'29.88"	32°35'38.05"	174/64	9.5	295.1	8.1	15.7	15.2	28.5	10.6	48.4	8.0	5.2	22.1	8
WT15 ^D	35°01'29.88"	32°35'38.05"	200/41	7.8	292.6	4.7	9.9	9.2	56.2	7.5	140.2	4.7	5.2	22.1	8
WT16	35°02'32.22"	32°37'45.26"	173/59	8.7	302.4	9.5	24.4	16.1	52.0	9.4	53.5	9.2	5.9	26.5	6
WT17	35°01'46.97"	32°37'15.32"	172/57	4.5	296.4	14.1	16.9	26.1	21.2	17.0	31.1	13.9	6.3	29.7	5
WT18	35°01'41.99"	32°36'40.10"	167/55	6.4	300.1	3.4	8.1	6.7	188.9	4.0	263.5	3.4	5.2	22.1	8
WT19	35°00'24.65"	32°33'55.04"	195/37	10.4	277.5	4.7	8.7	9.1	61.1	7.1	142.9	4.7	5.2	22.1	8
WT20	35°00'24.65"	32°33'55.04"	187/41	7.2	285.7	5.7	-0.5	11.5	65.3	8.4	137.1	5.7	5.9	26.5	6
WT21	35°09'37.42"	32°35'37.56"	223/59	5.3	325.4	12.0	27.9	19.4	21.2	12.3	23.9	11.6	5.2	22.1	8
WT22	35°09'57.33"	32°35'30.63"	260/50	6.2	319.8	7.5	6.2	14.8	21.2	12.3	55.7	7.5	5.2	22.1	8
WT23	35°04'55.15"	32°37'55.68"	159/41	3.4	283.4	11.9	18.0	21.7	18.1	13.4	23.3	11.7	5.2	22.1	8
WT24	35°01'55.13"	32°38'09.95"	193/72	2.1	308.5	5.8	28.2	9.3	73.7	6.5	99.9	5.6	5.2	22.1	8
WT25	35°01'26.85"	32°36'15.08"	167/53	6.4	304.9	17.2	31.4	26.2	12.9	16.0	12.3	16.4	5.2	22.1	8
WT26	35°01'19.63"	32°34'45.69"	148/63	8.5	277.5	20.6	22.4	35.9	14.5	20.8	15.4	20.1	6.3	29.7	5
WT27	35°06'07.11"	32°37'53.82"	172/48	9.4	304.9	14.0	24.3	23.9	12.4	19.8	24.9	13.7	5.9	26.5	6
WT28	35°06'55.81"	32°37'33.77"	226/33	5.9	311.3	7.9	13.1	15.0	34.9	9.5	51.3	7.8	5.2	22.1	8

Table DR2. Net tectonic rotation solutions for sheeted dikes of the western Troodos ophiolite.

Site	Preferred solution						Alternate solution					
	Rotation axis		R	Sense	Initial dike		Rotation axis		R	Sense	Initial dike	
	Az	Plunge			Strike	Dip	Az	Plunge			Strike	Dip
<i>Northern domain</i>												
WT02	305.6	36.8	104.3	CW	322	90	069.9	30.5	42.1	CW	046	90
WT22	313.2	37.0	112.9	CW	321	90	070.7	39	52.6	CW	047	90
WT21	309.2	57.4	90.8	CW	312	90	113.8	4.1	64.8	CW	056	90
WT01	303.2	48.1	113.3	CW	300	90	110.7	8.4	56.7	CW	068	90
WT03	302.6	37.7	87.1	CW	322	90	079.1	8.4	43.3	CW	046	90
WT05	298.3	32.4	109.4	CW	301	90	081.3	2.6	51.9	CW	067	90
WT28	307.8	39.7	100.3	CW	299	90	096.0	02	68.0	CW	069	90
<i>Southern domain</i>												
WT27	303.9	49.9	70.7	CW	290	90	284.9	19.3	99.1	CCW	078	90
WT23	297.4	32.9	62.2	CW	294	90	269.9	23.2	97.6	CCW	074	90
WT07	299.9	16.4	111.1	CW	309	90	049.2	4.5	58.4	CW	060	90
WT20	319.4	23.9	59.9	CW	328	90	249.4	6.7	65.8	CCW	049	90
WT08	317.8	26.1	56.5	CW	310	90	263.6	13.9	93.0	CCW	058	90
WT16	308.1	53.5	56.8	CW	303	90	283.4	19.7	96.6	CCW	065	90
WT24	311.3	64.0	52.5	CW	323	90	286.4	13	73.9	CCW	045	90
WT17	318.4	46.1	49.8	CW	313	90	276.1	16.6	91.3	CCW	056	90
WT18	338.1	43.7	49.6	CW	313	90	275.8	11.8	100.0	CCW	055	90
WT12*	005.9	23.9	35.9	CW	347	90	249.3	4.9	57.8	CCW	021	90
WT14*	335.0	47.5	39.0	CW	324	90	273.7	15.4	85.4	CCW	044	90
WT25	295.8	53.8	69.1	CW	284	90	287.9	24.7	105.6	CCW	084	90
WT09	288.2	40.4	46.8	CW	308	90	274.6	29.4	91.2	CCW	060	90
WT26*	304.3	31.5	32.7	CW	309	90	270.1	27.9	106.4	CCW	059	90
WT11*	330.3	0.6	18.0	CCW	330	90	285.6	40.1	106.5	CCW	038	90
WT19	295.0	23.2	78.0	CW	309	90	252.8	18.2	66.2	CCW	059	90